J. Min. Metall. Sect. B-Metall. 59 (1) (2023) 91 - 100

Journal of Mining and Metallurgy, Section B: Metallurgy

CORROSION PROPERTIES OF ALUMINIZED 16Mo3 STEEL

B. Karpe [a*], K. Prijatelj [b], M. Bizjak [a], T. Kosec [b]

[a] University of Ljubljana, Faculty of Natural Sciences and Engineering, SI-1000 Ljubljana, Slovenia
[b] Slovenian National Building and Civil Engineering Institute, SI-1000 Ljubljana, Slovenia

(Received 27 September 2022; accepted 20 February 2023)

Abstract

Chromium-molybdenum steel (16Mo3) is widely used in petroleum, gas, automotive, and construction industries due to its good oxidation resistance and mechanical properties at moderately elevated temperatures. The aim of the research was to evaluate the corrosion susceptibility of 16Mo3 steel in hot rolled and aluminized states. Aluminization was performed by diffusion pack aluminization process at 900 °C / 2h and 730 °C / 4h, respectively. Electrochemical corrosion testing included measuring open circuit potential (EOCP), linear polarization resistance (LPR), potentiodynamic polarization, and electrochemical impedance spectroscopy (EIS) in potassium phosphate buffer (KH_2PO_4, pH = 7). Optical microscopy (OM), scanning electron microscopy (SEM), and energy dispersive X-ray spectroscopy (EDS) were used for surface layer microstructure characterization before and after corrosion tests. It was demonstrated that corrosion resistance of aluminized steel increased substantially. Corrosion properties were related to the structure and properties of intermetallic phase (FeAl, $FeAl_2$ and Fe_2Al_5) that formed on the surface of 16Mo3 steel.

Keywords: *Aluminide coatings; Aluminized steel; Aluminizing; Electrochemical corrosion investigation; 16Mo3 steel*

1. Introduction

Chromium-molybdenum steel (16Mo3 W.Nr. 1.5415, Table 1) has been widely used in the petroleum, chemical, and construction industries due to its good weldability, oxidation resistance, and mechanical properties at moderately elevated temperatures. It also has certain strength properties, such as guaranteed yield stress and creep resistance up to 500 °C. However, its main disadvantage is corrosion susceptibility. 16Mo3 steel is mainly used for components of steam boilers and pressure vessels, heat exchangers, header chambers, parts for chemical equipment, hot gas manifolds, bolts, flanges, screws, nuts, and coils in the petroleum, chemical and power processing industries and, thus, it is exposed to various chemicals and harsh environment. Its microstructure depends on the processing method and the cooling rate during quenching. In the soft annealed condition, it has a ferrite-pearlite microstructure, while at higher cooling rates a bainitic or martensitic microstructure can also be obtained [1, 2].

Aluminization of steels and superalloys has found a wide application in the hot corrosion and oxidation protection. A literature searches on corrosion testing of aluminized steel revealed that only very specific types of corrosion, such as hot temperature corrosion or erosion corrosion, have been studied [3, 4]. Hot temperature corrosion study was performed for aluminized steel 9-12% Cr P91, estimating the thickness of corrosion products formed [3]. Another corrosion estimation was performed using scanning vibrating electrode technique (SVET) to estimate the protective behavior of aluminized steel [4]. Hot dip aluminized steel Type 2 (ASTM 929) was also tested for its corrosion resistance in limestone backfill using a special electrochemical setup [5]. Another corrosion study on aluminized steel suggested that aluminized steel had lower corrosion potential and stronger anodic activity in seawater, with chloride ions incorporated into the corrosion film [6].

Pack aluminization of superalloys is a widely used method for forming aluminide layers on turbine blades of aircraft gas turbines [7]. It is a diffusion-controlled process in which the work pieces are embedded in a powder mixture of aluminum (or its alloys with chromium, silicon, iron, platinum etc.) as the active component, alumina Al_2O_3 as an inert filler that prevents the mixture from sintering, and a halide activator (NH_4Cl, $AlCl_3$, AlF_3, etc.) and annealed between 500 °C and 1100 °C [8-13]. During the

*Corresponding author: blaz.karpe@ntf.uni-lj.si

https://doi.org/10.2298/JMMB220927008K

CC BY SA

heating of the container with the saturation mixture and the aluminized parts, first the activator (NH_4Cl at 340 °C) decomposes by the following reactions [7]:

$$NH_4Cl \leftrightarrow NH_3 + HCl \quad (1)$$

$$2NH_3 \leftrightarrow N_2 + H_2 \quad (2)$$

The hydrogen chloride (HCl) then reacts with aluminum to form aluminum chloride:

$$6HCl + 2Al \leftrightarrow 2AlCl_3 + 3H_2 \quad (3)$$

In addition, aluminum chlorides react with aluminum by one of the following reactions:

$$AlCl_3 + 2Al \leftrightarrow 3AlCl \quad (4)$$

$$*2AlCl_3 + Al \leftrightarrow 3AlCl_2 \quad (5)$$

*$AlCl_2$ is predominant at temperatures >1200K

Gaseous aluminum chlorides of lower valence diffuse through the powder mixture to the work piece surface, where disproportionation reactions occur, resulting the formation of aluminides on surface and gaseous aluminum chlorides of higher valence:

$$3AlCl + 2nFe \leftrightarrow AlCl_3 + 2Fe_nAl_m \quad (6)$$

$$3AlCl_2 + nFe \leftrightarrow 2AlCl_3 + Fe_nAl_m \quad (7)$$

The aluminum chlorides ($AlCl_3$) return to the powder mixture, where they react again with aluminum, continuing the previous reactions [7]. The result of this interaction is that aluminum chlorides ($AlCl_3$) are not consumed in the aluminization process. The aluminization process occurs due to the thermodynamic equilibrium shift in the gas mixture resulting from the absorption of aluminum and its diffusion into the processed metal. The results of aluminization, such as the dimensions and composition of the coatings formed, depend not only on the amount of aluminum chloride in the mixture, but also on the rate of its delivery to the saturated surface, the rate of surface reaction, the rate of the reaction product discharge to the mixture, and the rate of aluminum diffusion in the coating being formed, which makes quantitative analysis extremely complicated. Therefore, in practice, the aluminization process is characterized experimentally by the relationship between the composition of the powder mixture and the properties of the coating at a given annealing temperature [7-13].

In this study, two different aluminization processes were performed on 16Mo3 steel. Electrochemical characterization was conducted to determine the differences in corrosion properties of two different aluminized surfaces and 16Mo3 steel as reference material. Corrosion evaluation was supported by the study of the surface morphology and extent of corrosion processes using optical and electron microscopy.

2. Experimental

2.1. Materials and methods

All specimens (16Mo3 –®Siqual 5415 Metal Ravne) were cut longitudinally as strips from hot-rolled, unused tubes, milled, turned, ground, and polished to final dimensions (Φ 15 mm, h = 2 mm) and ultrasonically cleaned in alcohol. Pack aluminization was performed in a lidded ceramic container by embedding the samples in a powder mixture (pack) of 6 wt% Al (diffusion element), 3 wt% NH_4Cl (activator), 91 wt% Al_2O_3 (inert filer) and annealed in a tube furnace in Ar + 7 vol.% H_2 gas stream (®Inoxline H7, Messer) at 730 °C for 4 hours or at 900 °C for 2 hours. The heating and cooling rates were 10 °C min^{-1} in all cases. The powder mixture was prepared in the Turbula mixer from 99.8% pure Al powder (size 64 ± 32 μm; Exotherm - IT d.o.o), NH_4Cl salt (Sigma Aldrich) and 99.99% pure Al_2O_3 powder (size 62 ± 32 μm; Accumet Materials Co.).

Electrochemical measurements were performed at room temperature using a Gamry Reference 600+ potentiostat/galvanostat and Gamry Instruments Framework software, in a three-electrode cell in potassium phosphate buffer KH_2PO_4 with a stable neutral pH of 7. The test solution was chosen due to low solubility of aluminum oxide at pH 7 and thus allowing better differentiation of electrochemical properties of aluminized samples [14]. The standard Ag/AgCl reference electrode and a graphite counter electrode were used in all experiments. Minimum two replicates of each sample were measured electrochemically. Surface (working electrode) of the aluminized samples was cleaned by fine grinding (SiC 800) and gentle brushing in alcohol, with the aim to remove all the residue stuck on the surface after aluminization in powder mixture. The open circuit potential was measured after a one-hour stabilization period immediately after immersion of the sample in the electrolyte. Linear polarization measurements were made at ± 20 mV interval according to E_{OCP} with a rate of 0.1 mV s^{-1}. Electrochemical impedance spectroscopy (EIS) was performed in the frequency range from 65 kHz to 1 mHz with 7 points per decade and a sinusoidal excitation voltage of 10 mV. Potentiodynamic measurements were performed in the potential range from –250 mV (cathodic) to 1.2 V (anodic) according to E_{OCP}, with a scan rate of 1 mV s^{-1}, starting from the cathodic region. The cross-sections of the specimens for the microstructure observations

CC BY SA

were prepared with the classical metallographic preparation by grinding with SiC papers and polishing with 3 μm and 1 μm diamond suspension. The microstructure of the samples before and after aluminization, as well as the morphology of the corrosion surface, were studied using a Thermo Fisher Scientific Quattro S FEG and JEOL JSM-IT500LV electron scanning microscopes equipped with an EDX spectrometer for chemical analysis and Olympus BX61 optical microscope. Hardness measurements were performed using the Vickers Instron Tukon 2100B tester.

3. Results and Discussion

3.1. Characterization of aluminized 16CrMo3 steel

The microstructure of the 16Mo3 steel in the hot-rolled and aluminized states are presented in Figure 1. The microstructural images were taken in the center of the specimens, far enough away from the surface to be affected by aluminum diffusion. As can be seen, the 16Mo3 steel in the hot-rolled condition exhibited a ferrite-pearlite microstructure. After annealing at 730 °C for 4 hours, which was slightly above the A_{c1} temperature, partial spheroidization of the pearlite occurred, while the crystal grains size remained virtually the same (Figure 1 b). On the other hand, significant growth of crystalline grains occurred during annealing at 900 °C for 2 hours (Figure 1c). The hardness of the steel decreased with the annealing temperature of aluminization due to pearlite spheroidization and crystal growth (Table 2).

Figures 2 and 3 show the microstructures with aluminum and iron concentration profiles (EDS line analysis) of the specimen cross sections perpendicular to the surface after aluminization annealing. After aluminization at 730 °C for 4 hours, a three-layer microstructure developed: A 5 μm thick layer at the surface with a nearly constant Al concentration of 52 wt %, a 10 μm thick layer with a steep Al concentration gradient, and a 4 to 5 μm thick layer with a shallower Al concentration gradient. According to the Al-Fe phase diagram [14], the outermost layer consisted of an intermetallic Fe_2Al_5 phase, the middle layer consisted of a mixture of intermetallic Fe_2Al_5, $FeAl_2$, and FeAl phases, and the 1 to 2 μm thick inner layer of an α-Fe (ferrite) solid solution. After aluminization at 900 °C for 2 hours, a much thicker (55 μm) aluminum-enriched layer was formed: 30 μm thick layer with a constant Al concentration gradient and an inner layer with a steep local change in Al concentration, indicating a multiphase structure. According to the Al-Fe phase diagram, the outermost layer consisted of an intermetallic FeAl and $FeAl_2$ phases, while the inner layers consisted of an intermetallic phase Fe_3Al and α-Fe solid solution (Fig. 4), visible as ferrite grain zone beneath aluminide layers. Hot oxidation products were also found on surface (Al_2O_3). It should be emphasized that the oxides formed locally on the surface and not in the form of a thin continuous film. The partial oxidation occurred because the furnace was only purged with a gas stream and not really evacuated, which did not prevent partial oxidation due to desorbed oxygen from the powder mixture. In addition, most of the oxide

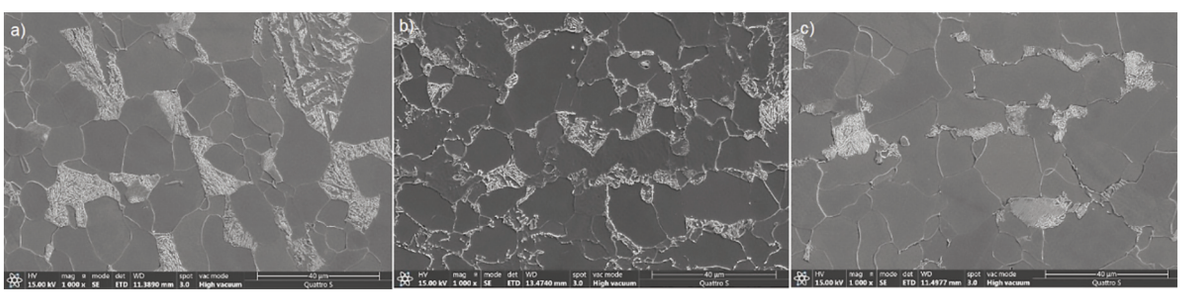

Figure 1. *Microstructure of the 16Mo3 steel in the core of the sample: a) hot rolled, b) aluminized at 730 °C/4h, c) aluminized at 900 °C/2h*

Table 1. *Chemical composition of 16Mo3*

El.	C	Si	Mn	Mo	Cu	S	N	P	Ni	Fe
wt.%	0.16	0.32	0.62	0.31	0.21	0.007	0.21	0.025	0.011	Bal.

Table 2. *Hardness of the 16Mo3 steel before and after aluminization*

16Mo3 condition	Hardness- HV0.3/St. deviation
Hot rolled	159.7/2.3
A730 °C/ 4 h	142.3/4.61
A900 °C/ 2 h	130.3/2.51

CC BY SA

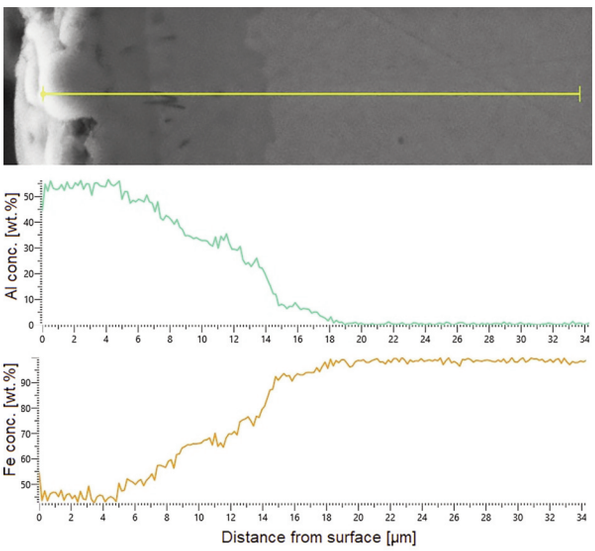

Figure 2. *Aluminum and Iron concentration profile perpendicular to 16Mo3 steel aluminized surface. Aluminized at 730 °C/4h, SEM-EDX line analysis*

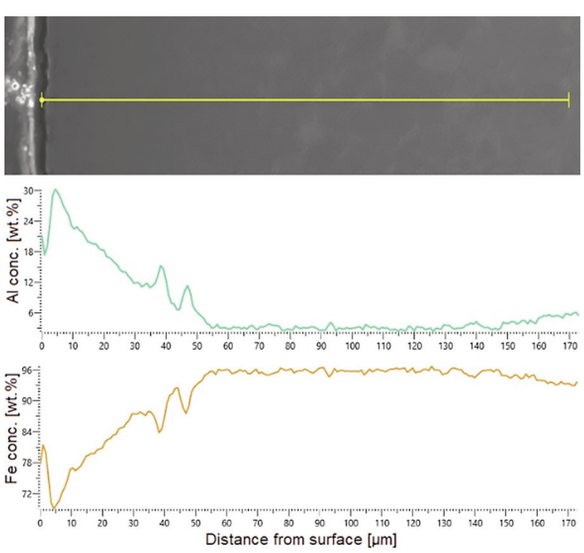

Figure 3. *Aluminum and Iron concentration profile perpendicular to 16Mo3 steel aluminized surface. Aluminized at 900 °C/2h, SEM-EDX analysis*

particles were removed by fine grinding prior to the electrochemical tests, so that in our opinion the small area fraction still covered with oxides did not significantly affect the measurement results.

3.2. Electrochemical measurements

The open-circuit potential of the hot-rolled and aluminized 16Mo3 steel samples was recorded during a 1-h immersion in phosphate buffer. As can be seen in Figure 5, aluminized samples exhibited less negative E_{OCP} values compared to untreated, hot-rolled 16Mo3 steel (-0.72 and - 0.73 V). Samples aluminized at 730 °C for 4 hours had the highest E_{OCP} values (-0.34 and -0.43 V), followed by samples aluminized at 900 °C for 2 hours (-0.38 and -0.41 V). The differences in E_{OCP} values were due to oxide films that formed on the surface of different intermetallic phases. The samples aluminized at 730 °C had predominantly an intermetallic Fe_2Al_5 phase on the surface, while the outermost layer of the samples aluminized at 900 °C consisted of oxides, and $FeAl_2$, FeAl intermetallic phases.

To determine the polarization resistance (R_p), the linear polarization measurements were performed in an interval of ± 10 mV versus E_{OCP} at a rate of 0.1

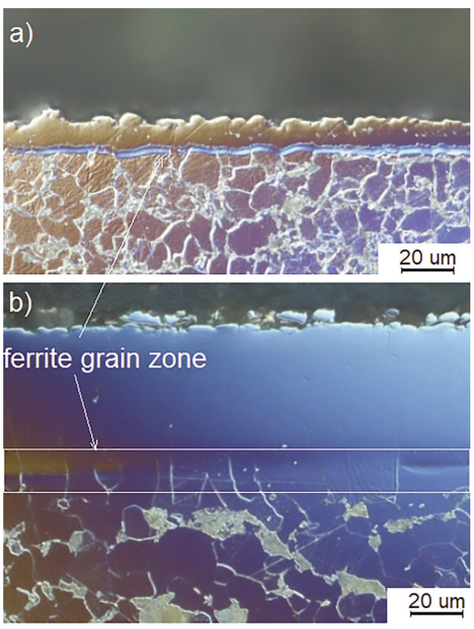

Figure 4. *Microstructure of aluminized 16Mo3 steel surface cross section: a) at 730 °C/4h, b) at 900 °C/2h, (OM- polarized light)*

mV s^{-1}. The lowest values of polarization resistance were measured on untreated, hot-rolled 16Mo3 steel samples, while aluminized samples exhibited much higher polarization resistance, indicating higher corrosion resistance of the aluminized samples (Fig. 6, Table 3) [15-19].

Compared to hot-rolled 16Mo3 steel, approximately 200–300 times higher corrosion resistance was measured on samples aluminized at

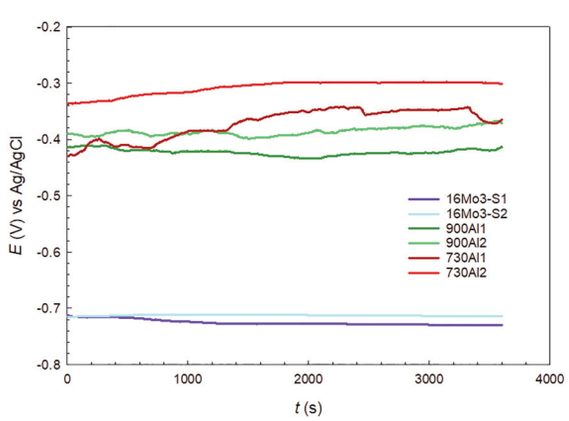

Figure 5. *Open circuit potential measurement plots in KH_2PO_4 buffer (pH = 7) of 16Mo3 steel in hot rolled and aluminized (730 °C/4h and 900 °C/2h) state*

730 °C, where Fe_2Al_5 intermetallic phases had formed. On samples that were aluminized at 900 °C, 65–90 times higher polarization resistance was

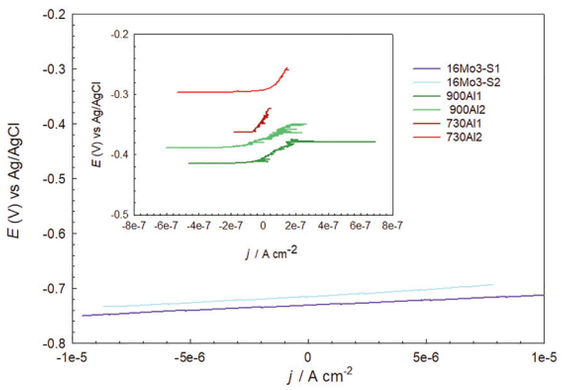

Figure 6. *Linear polarization measurement plots in KH_2PO_4 buffer (pH = 7) of 16Mo3 in hot rolled and aluminized (730 °C/4h and 900 °C/2h) state*

measured (Table 4), which reflect less corrosion resistant oxide film that formed on $FeAl_2$ and FeAl intermetallic phases.

The electrochemical impedance spectroscopy (EIS) measurements were also performed under the free-corrosion system conditions. Figure 7 shows the

Table 3. *Polarization resistance of hot rolled and aluminized 16Mo3 samples in KH_2PO_4 buffer, pH = 7*

Sample	E_{OCP} /[V]	R_p /[kΩ cm^2]
16Mo3 - S1	–0.731	2.19
16Mo3 - S2	–0.715	2.79
16Mo3 - 900Al1	–0.405	197
16Mo3 - 900Al2	–0.380	144
16Mo3 - 730Al1	–0.368	680
16Mo3 - 730Al2	–0.302	457

Nyquist and Bode diagrams in the frequency range from 65 kHz to 1 mHz, and Table 3 provides the absolute values of the impedance at the lowest measured frequency of 1 mHz. Impedance response of hot-rolled, untreated 16Mo3 steel samples was the lowest with low frequency tail pointing at dissolution of the surface film. Samples aluminized at 730 °C had the highest impedance, followed by samples aluminized at 900 °C. Aluminized samples also showed an increase in phase angle maximum and had much larger diameter of capacitance loop, indicating thicker and more compact surface passivation layer and, therefore, better corrosion resistance [19, 20].

Potentiodynamic measurements were performed in the potential range starting from -250 mV (cathodic region) up to 1.2 V (anodic region) versus E_{OCP} with a scan rate of 1 mV/s. Potentiodynamic curves, presented as a semi-logarithmic plot, are shown in

CC BY SA

Table 4. *Values of absolute impedance at frequency 1 mHz for hot rolled and aluminized 16Mo3 steel*

Sample	|Z| [kΩ cm^2]
16Mo3 - S1	3.44
16Mo3 - S2	4.77
900Al1	229
900Al2	209
730Al1	287
730Al2	264

(indicated by arrow in Figure 9). If positive hysteresis was observed with higher current density, a tendency to local forms of corrosion could be expected, while negative hysteresis resulted in lower current densities and good re-passivation properties. As shown in Figure 9, the sample aluminized at 900 °C, exhibited negative hysteresis and a larger difference between the corrosion potential E_{corr} and re-passivation potential E_{rep}, indicating good re-passivation properties. The sample aluminized at 730 °C exhibited positive hysteresis, a narrower anodic region with constant current density up to breakdown potential E_b at 0.02 V. Positive hysteresis indicated a

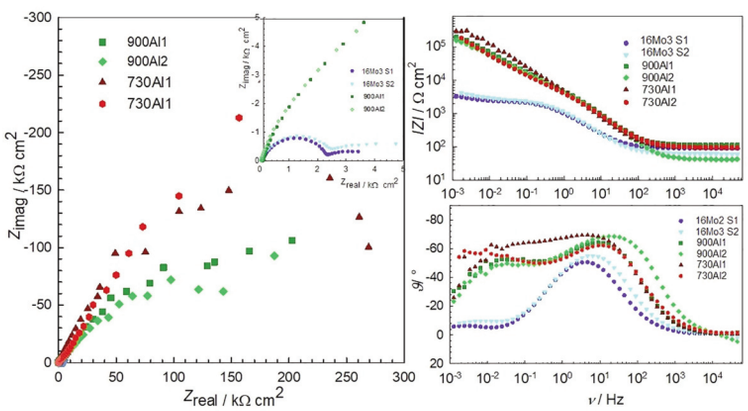

Figure 7. *Nyquist diagram (left) and Bode diagrams (right) for 16Mo3 steel in hot rolled and aluminized state in KH_2PO_4 buffer, pH = 7*

Figure 8. Higher corrosion potential E_{corr} and two orders of magnitude lower corrosion current density j_{corr} indicated much better corrosion resistance of aluminized 16Mo3 steel (Table 5), while instability of measured anodic current density at higher potentials and poorer repeatability between samples of the same aluminization process indicated inhomogeneity of the surface layer [17-19].

Cyclic polarization measurements (Table 6) were also performed on aluminized samples. By measuring the cyclic polarization, the information on repassivation properties of the formed coatings was obtained. In this test, potential was scanned from cathodic region up to anodic region, where at defined current density (1 mA cm^{-2}) the scan was reversed

tendency to pitting and crevice corrosion [21]. This difference occurred due to different intermetallic phases formed on the surface at different aluminization temperatures. The outer layer of coating formed during aluminization at 730 °C / 4h was composed of the intermetallic phase Fe_2Al_5, while after aluminization at 900 °C/2h its composition was heterogenic (FeAl, $FeAl_2$, oxides).

3.3. Surface morphology investigation

Figure 10 shows the macroscopic surface morphology of hot-rolled and aluminized 16Mo3 steel after electrochemical tests. General corrosion is the

Table 5. *Corrosion parameters of hot rolled and aluminized 16Mo3 steel in KH_2PO_4 buffer*

Sample	E_{corr} /[V] [V]	j_{corr}/[μA cm^{-2}]	E_b /[V]
16Mo3 - S1	–0.747	4.97	–0.368
16Mo3 - S2	–0.724	4.4	–0.388
16Mo3 – 900Al1	–0.438	0.051	0.243
16Mo3 - 900Al2	–0.401	0.064	0.267
16Mo3 - 730Al1	–0.420	0.043	–0.052
16Mo3 - 730Al2	–0.442	0.126	Not detected

CC BY SA

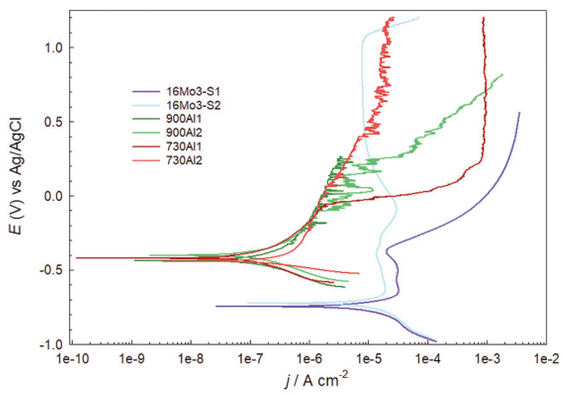

Figure 8. *Potentiodynamic polarization curve of 16Mo3 steel in hot rolled and aluminized state in KH_2PO_4 buffer, pH = 7*

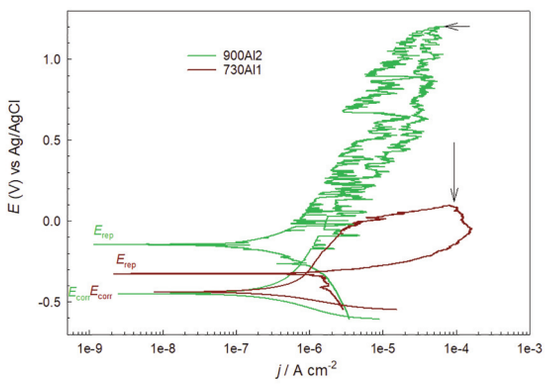

Figure 9*. Cyclic polarization curves in KH_2PO_4 buffer (pH = 7) of 16Mo3 steel aluminized at 900 °C/2h and 730 °C/4h*

Table 6. *Cyclic polarization measurement values of aluminized steel in KH_2PO_4 buffer*

16Mo3-aluminized	E_{corr} /[V]	E_b /[V]	E_{rep} /[V]
900Al2	–0.451	1.15	–0.143
730Al1	–0.436	0.02	–0.318

predominant type on the hot rolled steel sample, while in the case of the aluminized samples, pitting corrosion occurred only on samples with distinctive breakdown potential (900A2, 730A1). Detailed microscopic and chemical analysis (Figure 11) showed that the corrosion products, when they occurred on aluminized specimens, consisted mainly of elements of the potassium phosphate buffer surrounded by aluminum and iron oxides and hydroxides, regardless of the aluminization process used.

The corrosion rate was calculated using the parameters obtained from the linear polarization and potentiodynamic measurements. Table 7 shows the corrosion rate calculations for each steel sample. However, the calculated corrosion rates for the aluminized specimens should be treated with caution due to localized corrosion [22-26]:

$$j_{corr} = \frac{\beta_a \cdot \beta_c}{2.303 \cdot (\beta_a + \beta_c) \cdot R_p} \tag{8}$$

$$CR = K_1 \cdot \frac{j_{corr} \cdot EW}{\rho_i} \tag{9}$$

where K_1 = 3.272 μm g μA^{-1} cm^{-1} $year^{-1}$, ρ_i density of the steel (7,85 g cm^{-3}) or coating on the surface, EW alloy equivalent weight.

$$EW = \frac{1}{Q} = \frac{1}{\sum \frac{z_i \cdot w_i}{M_i}} \tag{10}$$

where z_i (z_{Fe} = 2; z_{Al} = 3) is valence number, w_i mass fraction and M_i atomic weight of i^{th} element of the alloy. For aluminized specimens, the mass fractions of Al and Fe (30/70 wt.% Al/Fe for the specimens aluminized at 900°C/2h and 52/48 wt.% Al/Fe for the specimens aluminized at 730 °C/4h, SEM-EDS) and the densities of the intermetallic

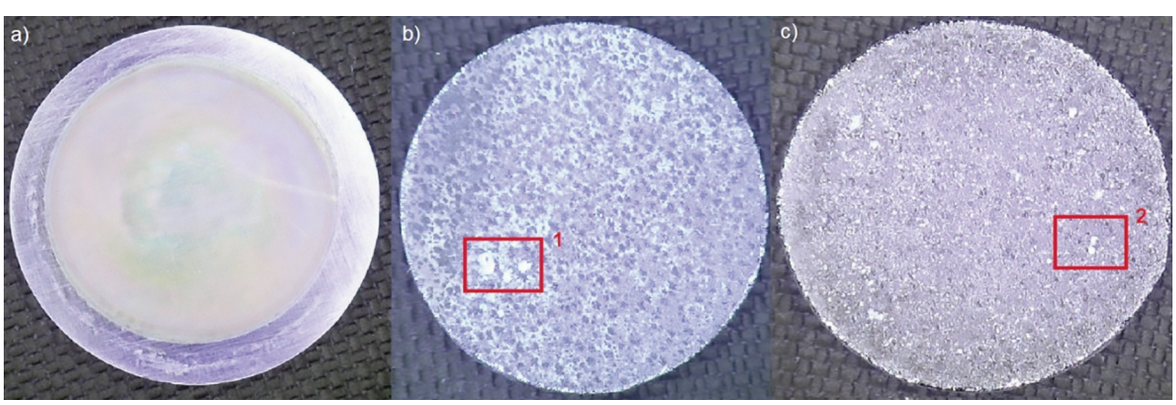

Figure 10. *Surface of the 16Mo3 steel after electrochemical investigation in phosphate buffer, a) hot rolled, b) aluminized at 730 °C/4h, c) aluminized at 900 °C/2h*

CC BY SA

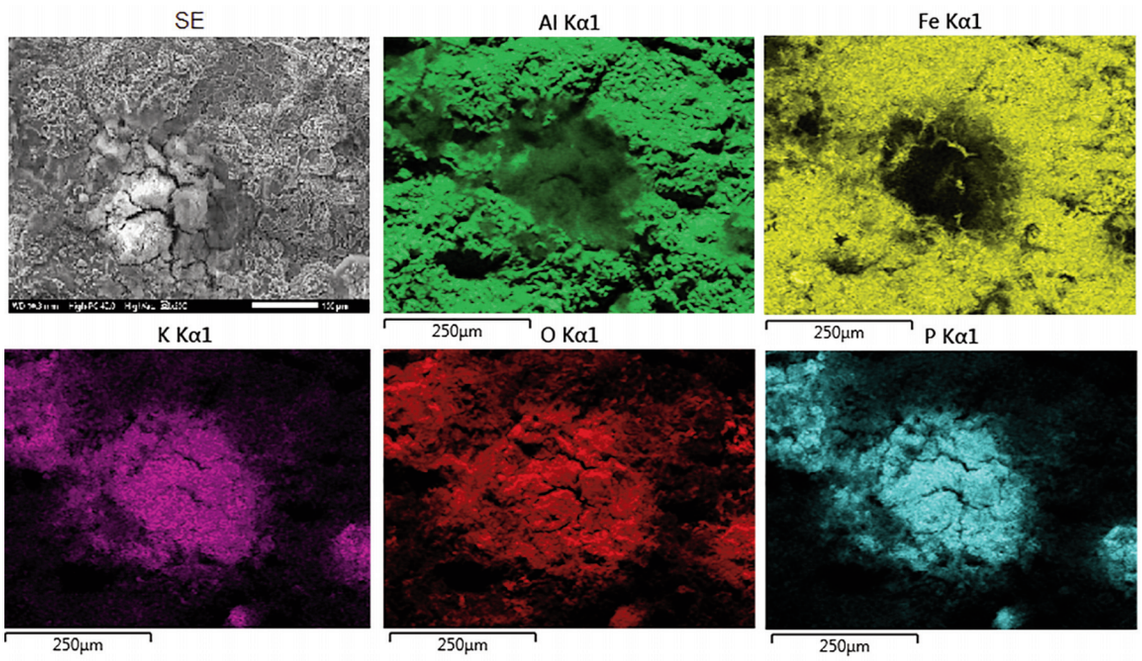

Figure 11. *Secondary electron imaging and specific element distribution of corrosion product after electrochemical measurements in phosphate buffer for16Mo3 steel aluminized at 900°C/2h*

phases FeAl (6,62 g cm^{-3}) and Fe_2Al_5 (3,96 g cm^{-3}) were considered.

Table 7. *Calculated corrosion rates of hot rolled and aluminized 16Mo3 steel in KH_2PO_4 buffer*

Sample	CR (LPR)/[µm/year]	CR (PD) /[µm/year] (CR [µm/year])
16Mo3-S1	137.7	57.8
16Mo3-S1	108.1	51.2
900Al1	1.11	0.43
900Al2	1.52	0.54
730Al1	0.42	0.47
730Al2	0.63	1.39

4. Conclusions

The aim of the research was to enrich the surface of selected 16Mo3 steel with aluminum to form coating consisted from various FexAly intermetallic phases. The annealing temperature during pack aluminization, as well as pack composition, determine the type of the aluminide phase formation and had also a major influence on Al diffusion depth. During aluminization at 730 °C / 4h, multilayer coating formed, with the Fe_2Al_5 intermetallic phase as the outermost layer, while during aluminization at 900 °C / 2h, the outermost layer consisted from FeAl and $FeAl_2$ intermetallic phases. Electrochemical measurements showed that aluminide layers improved corrosion resistance compared to 16Mo3 base steel. Corrosion properties of the aluminized layers varied to a small extent on the type of intermetallic phase. The intermetallic Fe_2Al_5 phase had higher polarization resistance, but its main disadvantage was the positive hysteresis of cyclic polarization, indicating a tendency to pitting corrosion. In addition, it was brittle and prone to spalling if the product was exposed to thermal cycling [7, 27]. On the other hand, the intermetallic FeAl coating had a negative hysteresis of the cyclic polarization curve and a larger difference between the corrosion potentials of the forward polarization E_{corr} and the reverse polarization $E_{corr,rev}$ and, thus, a much higher prospect of corrosion protection coating. Unfortunately, significant grain growth during high-temperature aluminizing (900 °C / 2h) and thicker ferrite zone led to a reduction in the yield and tensile strength of the steel (Hall-Petch relationship). The recommended aluminide coating thickness depended on both the operating conditions of the application and the alloy used. Aluminide film with the thicknesses of up to 200 µm was reported as suitable for certain applications [3, 7], but usually thinner coatings were applied. The oxidation and corrosion resistance at high temperatures was directly proportional to the film thickness used; on the other hand, thick films were more prone to cracking due to thermally induced stresses. In addition, the thickening

rate of the coating decreased over time, while prolonged exposure to high temperatures during the aluminizing process degraded the mechanical properties of the substrate itself due to crystal grain growth. Future work will focus on aluminization at lower temperatures and with much lower aluminum activity in the powder mixture (pack) to form intermetallic FeAl and $FeAl_2$ phases on the surface and prevent excessive ferrite zone thickening and crystal grain coarsening.

Acknowledgments

This research was conducted within research core program P2-0273, (ARRS, Slovenian research agency). The help of Mirjam Bajt Leban with SEM/EDS analysis is greatly acknowledged.

Author contribution

Writing-original draft, Data curation, Conceptualization: Blaž Karpe, Funding acquisition, Writing-review & editing, Supervision: Tadeja Kosec, Investigation, Data curation: Klara Prijatelj, Validation: Milan Bizjak

Data availability

The data used to support the findings of this study are available from the corresponding author upon request.

Conflict of interest

The authors declare that they have no known competing financial interests or personal relationships that could have appeared to influence the work reported in this paper.

References

[1] M. Hofmann, H. Biermann, Static and cyclic deformation behavior of the ferritic steel 16Mo3 under monotonic and cyclic loading at high temperatures, Steel Research International, 83 (7) (2012) 631-636. https://doi.org/10.1002/srin.201100238

[2] M. Özdemir, H. Hakan Gökmeşe, V. Yilmaz, The development of microstructure and mechanical properties of Cr-Mo high temperature steel in different heat-treated-state, Journal of Basic and Applied Research International, 11 (4) (2015) 198-205. https://doi.org/10.5281/zenodo.7688358

[3] J. Metsäjoki, E. Huttunen-Saarivirta, T. Lepistö, Elevated-temperature corrosion of uncoated and aluminized 9–12% Cr boiler steels beneath KCl deposit, Fuel, 133 (2014) 173-181. https://doi.org/10.1016/j.fuel.2014.05.017

[4] B. Lemmens, Y. Gonzalez Garcia, B. Corlu, J. De Strycke, I. De Graeve, K. Verbeken, Study of the electrochemical behaviour of aluminized steel, Surface and Coatings Technology, 26 (2014) 34-38. https://doi.org/10.1016/j.surfcoat.2014.06.064

[5] M. Akhoondan, A. Sagüés, Corrosion of aluminized steel in aggressive natural water, ECS Transactions - The Electrochemical Society, 4 (19) (2013) 25-35. https://doi.org/10.5006/0879

[6] C. Liang, J. Wei, S. Li, R. Zheng, Electrochemical behavior of aluminized steel in seawater environment, Journal of Electrochemistry, 10 (4) (2004) 435-439.

[7] Y. Tamarin, Protective coatings for turbine blades, ASM International, 2002, p. 247

[8] Y. Matsuoka, Y. Matsunaga, K. Nakagawa, Y. Tuda, S. Taniguchi, Growth behaviour of coatings formed by vapour phase aluminizing using Fe-Al pellets of varying composition, Journal of the Japan Institute of Metals, 47 (9) (2006) 2341-2347. https://doi.org/10.2320/matertrans.47.2341

[9] Z. Xiang, P. Datta, Effects of pack composition on the formation of aluminide coatings on alloy steels at 650 °C, Journal of Materials Science, 40 (8) (2005) 1959-1969. https://doi.org/10.1179/026708304225022232

[10] Q. Wang, X. Leng, T. Yang, J. Yan, Effects of Fe-Al intermetallic compounds on interfacial bonding of clad materials, Transactions of Nonferrous Metals Society of China, 24 (1) (2014) 279-284. https://doi.org/10.1016/S1003-6326(14)63058-2

[11] A. Naji, M.C. Galetz, M. Schutze, Improvements in the thermodynamic and kinetic considerations on the coating design for diffusion coatings formed via pack cementation. Materials and Corrosion, Institute dechema, 66 (9) (2015) 863-868. https://doi.org/10.1002/maco.201407810

[12] M. Pourbaix, Atlas of electrochemical equilibria in aqueous solutions, National association of Corossion Engineers, Huston, 1974, p. 648

[13] M.M. Barjesteh, S.M. Abassi, K. Zengeneh Madar, K. Shirvani, Creep rupture properties of bare and coated polycrystalline nickel-based superalloy Rene®80, Journal of Mining and Metallurgy, Section B: Metallurgy, 57 (3) (2021) 401 – 412. https://doi.org/10.2298/JMMB201203036B

[14] H. Sina, J. Corneliusson, K. Turba, S. Iyengar, A study on the formation of iron aluminide (FeAl) from elemental powders, Journal of Alloys and Compounds, 636 (2015) 261-269. https://doi.org/10.1016/j.jallcom.2015.02.132

[15] F. Mansfeld, Fundamental aspects of linear polarization technique-the early days, Journal of Solid State Electrochemistry, 13 (2009) 515-520. http://dx.doi.org/10.1007/s10008-008-0652-x

[16] A. Berradja, Electrochemical techniques for corrosion and tribocorrosion monitoring: Methods for the assessment of corrosion rates, IntechOpen, Leuven, (2019). https:/doi: 10.5772/intechopen.85392

[17] S. Papavinasam, Electrochemical polarization techniques for corrosion monitoring: Chapter 3. In: Metals and Surface Engineering, Yang L (ed.) Elsevier, Carson City, 2008, 49-85.

[18] W. Choi, H. Shin, J.M. Kim, Modelling and applications of electrochemical impedance spectroscopy (EIS) for lithium ion batteries, Journal of Electrochemical Science and Technology, 11 (1) (2020) 1-13. https://doi.org/10.33961/jecst.2019.00528

[19] Y. Shi, X.Q. Liu, Z.I. Liu, H.J. Xie, Y.H. Wang, J. Li,

CC BY SA

Effect of Zn on corrosion behaviour of Mg-Y-Zn alloys, Journal of Mining and Metallurgy, Section B: Metallurgy, 58 (1) (2022) 51-61. https://doi.org/10.2298/JMMB210525048S

[20] S. Esmailzade, M. Aliofkhazraei, Interpretation of cyclic potentiodynamic polarization test results for study of corrosion behavior of metals: A Review, Protection of Metals and Physical Chemistry of Surfaces, 54 (2016) 976-989. https://doi.org/10.1134/S207020511805026X

[21] W. M. Lu, T.J. Pan, Y. Niu, Accelerated corrosion of Fe–xCr–10Al alloys containing 0–20 at% Cr induced by sulphur and chlorine in a reducing atmosphere at 600 °C, Oxidation of Metals, 69 (2008) 63–76. https://doi.org/10.1007/S11085-007-9083-9I.

[22] D.V. Lakshmi, P.S. Babu, L.R. Krishna, R. Vijay, D. S. Rao, G. Padmanabham, Corrosion and erosion behaviour of iron aluminide (FeAl(Cr)) coating deposited by detonation spray technique, Advanced Powder Technology, 32 (2021) 2192-2201. http://doi.org/10.1016/j.apt.2021.04.032

[23] Y. Alipour, P. Henderson, P. Szakálos, The effect of a nickel alloy coating on the corrosion of furnace wall tubes in a waste wood fired power plant, Materials and Corrosion 65 (2), (2014) 217-225. https://doi.org/10.1002/maco.201307118

[24] A. Talus, Y. Alipour, R. Norling, P. Henderson, Effect of sewage sludge addition on initial corrosion of16Mo3 and 310S when exposed in a used wood fired boiler, Materials and Corrosion, 67 (7) (2016) 683-692. https://doi.org/10.1002/maco.201508693

[25] Standard Practice for Calculation of Corrosion Rates and Related Information from electrochemical Measurements, ASTM G102-89R15E01, USA. http://www.astm.org/cgi-bin/resolver.cgi?G102-89R15E1

[26] I. Maj, S. Kalisz, A. Szymajda, G. Łaska, K. Gołombek, The influence of cow dung and mixed straw ashes on steel corrosion, Renewable Energy, 177 (2021) 1198-1211. https://doi.org/10.1016/j.renene.2021.06.019

[27] C.T. Liu, E.P. George, Intermetallics: Environmental embrittlement, Encyclopedia of Materials, Science and Technology, (2001) 4181 – 4186. https://doi.org/10.1016/B0-08-043152-6/00735-X

KOROZIVNA SVOJSTVA ČELIKA 16Mo3 OBLOŽENOG ALUMINIJUMOM

B. Karpe [a*], K. Prijatelj [b], M. Bizjak [a], T. Kosec [b]

[a] Univerzitet u Ljubljani, Fakultet za prirodnjačke i tehničke nauke, SI-1000 Ljubljana, Slovenija
[b] Slovenački nacionalni institut za građevinarstvo, SI-1000 Ljubljana, Slovenija

Apstrakt

Čelik legiran hromom i molibdenom (16Mo3) se koristi u naftnoj, gasnoj, automobilskoj i građevinskoj industriji zbog dobre otpornosti na oksidaciju, kao i mehaničkih svojstava na umereno povišenim temperaturama. Cilj istraživanja je procena podložnosti koroziji čelika 16Mo3 u toplovaljanom stanju i kada je obložen aluminijumom. Aluminizacija je izvedena difuzijom aluminijuma na 900 °C / 2h i 730 °C / 4h. Ispitivanje elektrohemijske korozije podrazumevalo je merenje potencijala otvorenog kola, otpora linearne polarizacije, potenciodinamičke polarizacije i spektroskopiju elektrohemijske impendanse u puferskom sistemu kalijum fosfata (KH_2PO_4, pH = 7). Optička mikroskopija, SEM i EDS su korišćeni za karakterizaciju mikrostrukture površinskog sloja pre i posle ispitivanja korozije. Rezultati su pokazali da je otpornost na koroziju čelika obloženog aluminijumom značajno povećana. Koroziona svojstva su povezana sa strukturom i osobinama intermetalne faze (FeAl, $FeAl_2$ i Fe_2Al_5) koja se formirala na površini 16Mo3 čelika.

Ključne reči: *Aluminidne prevlake; Čelik obložen aluminijumom; Aluminizacija; Ispitivanje elektrohemijske korozije; 16Mo3 čelik*

CC BY SA